8

Nonreciprocal Phenomena on Reflection of Terahertz Radiation off Antiferromagnets

T. Dumelow[1], J. A. P. da Costa[1], F. Lima[2] and E. L. Albuquerque[2]
[1]*Universidade do Estado do Rio Grande do Norte*
[2]*Universidade Federal do Rio Grande do Norte*
Brazil

1. Introduction

There are a number of ways that reciprocity principles in optics may be affected by the presence of a static magnetic field (Potton, 2004). A classic example is Faraday rotation in which a plane polarised electromagnetic beam propagating through a suitable medium is rotated in the presence of a static magnetic field along the direction of propagation. The handedness of this rotation depends on the propagation direction, a nonreciprocal effect usefully applied to the construction of optical isolators (Dötsch et al., 2005). Nonreciprocal effects of this type are closely related to the idea that magnetic fields break time reversal symmetry. Similar nonreciprocal phenomena can occur, in various guises, on reflection off a semi-infinite sample. We discuss such behaviour in the present chapter, in the context of reflection off antiferromagnetic materials. In contrast to nonreciprocal phenomena based on the Faraday effect, our interest is in the Voigt geometry, in which the static magnetic field is perpendicular to the direction of propagation. We consider the well established phenomena of nonreciprocity in the intensity and phase of oblique incidence radiation, but concentrate mainly on recent developments on nonreciprocal power flow and finite beam effects.

We restrict discussion to the simple two dimensional geometry shown in Figure 1. Radiation is reflected, in the *xy* plane, off a semi-infinite sample, isotropic in this plane, in the presence of a static magnetic field $\mathbf{B}_0$ along *z* (into the page). Note that, in this configuration, we do not have to worry about polarisation effects, since there is no mixing between s-polarised (electromagnetic **E** field component along *z*) and p-polarised (electromagnetic **H** field component along *z*) radiation.

Now compare Figure 1(a) to Figure 1(b), in which the sign of the incident angle has been reversed. In the absence of the magnetic field ($\mathbf{B}_0 = 0$), we can consider Figure 1(b) as the mirror reflection of Figure 1(a) through the *yz* plane, so we expect no change in the reflection behaviour. In terms of the incident and reflected beam signals, this is a trivial example of the Helmholtz reciprocity principle, which, in the present context, can be interpreted as saying that, in the absence of magnetic fields, an interchange of source and detector should not affect the signal received by the detector (Born & Wolf, 1980). When $\mathbf{B}_0$ is nonzero, however, the mirror reflection of Figure 1(a) through the *yz* plane no longer leads to Figure 1(b), as one might expect. The essential point here is that the static magnetic field $\mathbf{B}_0$ is an axial vector, and a mirror symmetry operation through the *yz* plane would therefore involve reversing the direction of this field, so that it would come out of the page (Scott & Mills, 1977). In fact

Source: Recent Optical and Photonic Technologies, Book edited by: Ki Young Kim,
ISBN 978-953-7619-71-8, pp. 450, January 2010, INTECH, Croatia, downloaded from SCIYO.COM

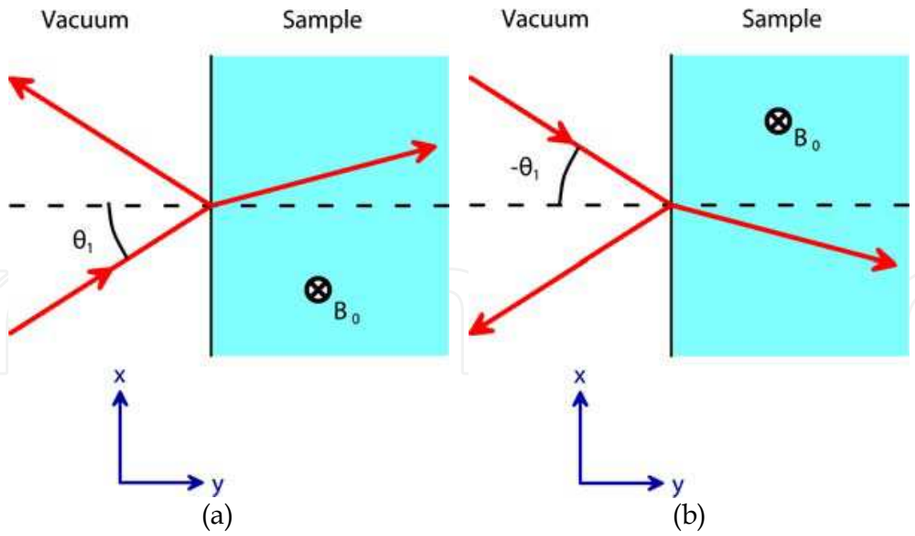

Fig. 1. Reflection geometry, showing interchange of incident and reflected beams.

there is no symmetry operation that leads us from Figure 1(a) to Figure 1(b), and the two figures are not equivalent. Nonreciprocal behaviour is thus, in principle, possible. Whether or not it occurs in practice, however, depends on the material properties of the sample.

In the present chapter we consider nonreciprocity associated with reflection off a simple uniaxial antiferromagnet. In this case the static field represented by $\mathbf{B}_0$ in Figure 1 is an external field, since an antiferromagnet has no intrinsic macroscopic magnetic field. We consider a geometry in which the anisotropy associated with the spin directions, along with the external field $\mathbf{B}_0$, is perpendicular to the plane of incidence. This is equivalent to putting the anisotropy along z in Figure 1, thus leaving the antiferromagnet isotropic in the xy plane. The electric component of the electromagnetic field is along z and the magnetic component is in the xy plane (s-polarisation).

In considering nonreciprocity in the intensity and phase of the reflected beam, it is sufficient to simply consider the effect of interchanging the incident and reflected beams (i.e. reversing the sign of θ_1). However, we note that a rotation of Figure 1(b) around the y axis brings us back to Figure 1(a), but with the field direction reversed. It is therefore possible to consider nonreciprocity in terms of a change in optical behaviour when the external field direction is reversed. This turns out to be more convenient when considering nonreciprocal effects inside the antiferromagnet and finite beam effects. It is notable that some of the new phenomena under investigation in this chapter occur at normal incidence, so such a test is simpler to visualise in such cases than a test based on the configurations of Figure 1. Thus our general test for nonreciprocity will be to see what happens when we reverse the sign of B_0.

2. Antiferromagnet permeability

The crucial parameter that determines the nonreciprocal optical properties of antiferromagnets is the magnetic permeability in region of the magnon (or spin wave) frequencies (Mills & Burstein, 1974), which typically lie in the terahertz range. We think of an antiferromagnet as two interpenetrating sublattices having opposite spin directions. Waves consisting of spins precessing in opposite directions in the two sublattices are then possible, and magnons of this type can interact with electromagnetic radiation. Their

resonant frequencies are linked not only to the anisotropy field B_A that tends to align the spins along a preferred axis (the z axis in our coordinate system), but also to the interaction between the spins in the two sublattices. In the long wavelength limit (applicable to terahertz frequencies), and in the absence of any external field, the resonance frequency is given by

$$\omega_r = \gamma\left(2B_A B_E + B_A^2\right)^{1/2} \tag{1}$$

Here B_E is the exchange field representing the interaction between the spins of the opposing sublattices and γ is the gyromagnetic ratio. In the presence of an electromagnetic field whose **H** component lies in the xy plane, the induced magnetisation follows the direction of this field component, since the spins in the two sublattices precess in opposite directions with equal amplitudes. The permeability tensor $\boldsymbol{\mu}$ is thus diagonal and of the form

$$\boldsymbol{\mu} = \begin{pmatrix} \mu & 0 & 0 \\ 0 & \mu & 0 \\ 0 & 0 & 1 \end{pmatrix}. \tag{2}$$

The scalar quantity μ is given, at frequency ω, by

$$\mu = 1 + \frac{2\mu_0\gamma^2 B_A M_S}{\omega_r^2 - \omega^2 + i\omega\Gamma}. \tag{3}$$

where M_S is the sublattice magnetisation and Γ is a damping parameter.
In this study, we are interested in propagation of electromagnetic waves (strictly speaking polariton waves, since the waves include a contribution from the precessing spins in addition to that of the electromagnetic radiation) within the xy plane. We consider the electromagnetic **E** field component to be directed along z with the corresponding **H** field component in the xy plane. In this case, for plane waves of the form

$$\mathbf{E}(x, y, t) = \mathbf{E}_0 \exp\left[i\left(k_x x + k_{1y} y - \omega t\right)\right], \tag{4}$$

$$\mathbf{H}(x, y, t) = \mathbf{H}_0 \exp\left[i\left(k_x x + k_{1y} y - \omega t\right)\right], \tag{5}$$

the polaritons follow the familiar dispersion relation

$$k_x^2 + k_y^2 = \epsilon\,\mu k_0^2 \tag{6}$$

where k_x and k_y are wavevector components and ϵ is the dielectric constant of the medium. k_0 is the modulus of the free space wavevector, given by

$$k_0 = \frac{\omega}{c}. \tag{7}$$

In the presence of an external field $\mathbf{B}_0$ along the anisotropy axis, the two sublattices are no longer equivalent. This leads to two effects. Firstly, there are now two resonances instead of one and, secondly, the permeability tensor is no longer diagonal, but gyromagnetic. It thus takes the form (Mills & Burstein, 1974):

$$\boldsymbol{\mu} = \begin{pmatrix} \mu_1 & i\mu_2 & 0 \\ -i\mu_2 & \mu_1 & 0 \\ 0 & 0 & 1 \end{pmatrix}, \tag{8}$$

where

$$\mu_1 = 1 + \mu_0 \gamma^2 B_A M_S (Y^+ + Y^-), \tag{9}$$

$$\mu_2 = \mu_0 \gamma^2 B_A M_S (Y^+ - Y^-), \tag{10}$$

with

$$Y^{\pm} = \frac{1}{\omega_r^2 - \left(\omega \pm \gamma B_0 + i\Gamma\right)^2}. \tag{11}$$

The diagonal elements μ_1 do not depend on the sign of the applied field $\mathbf{B}_0$, but μ_2 changes sign when $\mathbf{B}_0$ is reversed. This is the basis of the nonreciprocal effects discussed in this chapter. The polariton dispersion relation (Equation 6) is now replaced by

$$k_x^2 + k_y^2 = \epsilon\, \mu_v k_0^2 \tag{12}$$

where μ_v is known as the Voigt permeability, and is given by

$$\mu_v = \frac{\mu_1^2 - \mu_2^2}{\mu_1}. \tag{13}$$

It is straightforward to see that μ_v does not depend on the sign of the external field B_0, so the polariton dispersion relation (Equation 12) is similarly unaffected. Thus polariton dispersion corresponding to propagation through an antiferromagnet (as bulk polaritons) is, in the present geometry, totally reciprocal. Nonreciprocal effects only occur in the presence of a surface, as in the case of reflection off an antiferromagnet (Camley, 1987).

3. Nonreciprocity in reflection of plane waves

3.1 Reflected intensity

As discussed in the introduction, we can regard reflectivity R as nonreciprocal if there is a change in reflected intensity when the incident and reflected beams are interchanged, i.e. $R(\theta_1) \neq R(-\theta_1)$ where θ_1 is the angle of incidence (see Figure 1), or, equivalently, when the applied field $\mathbf{B}_0$ is reversed, i.e. $R(\mathbf{B}_0) \neq R(-\mathbf{B}_0)$. The possibility of nonreciprocal reflectivity in the present geometry was first analysed using thermodynamic arguments (Remer et al., 1984; Camley, 1987; Stamps et al., 1991). This analysis shows that reflectivity should be reciprocal in the absence of absorption, but that it need not be in the presence of absorption. Here we demonstrate the same result explicitly in the case of reflection off a uniaxial antiferromagnet, using the arguments outlined by Abraha & Tilley (1996) and Dumelow et al. (1998).

We are interested in reflection from vacuum in s polarisation. The complex reflection coefficient r in this case can be easily worked out from the field continuity conditions at the vacuum/antiferromagnet interface. Written in terms of the **E** field component of the electromagnetic radiation, the complex reflection coefficient is given by

$$r = \frac{k_{1y}\mu_v - k_{2y} - ik_x(\mu_2 / \mu_1)}{k_{1y}\mu_v + k_{2y} + ik_x(\mu_2 / \mu_1)} \tag{14}$$

with a corresponding transmission coefficient

$$t = 1 + r = \frac{2k_{1y}\mu_v(\mu_2 / \mu_1)}{k_{1y}\mu_v + k_{2y} + ik_x(\mu_2 / \mu_1)}. \tag{15}$$

k_x is the in-plane component of the wavevector, which is continuous in both media and determined by the angle of incidence θ_1:

$$k_x = k_0 \sin\theta_1. \tag{16}$$

k_{1y} and k_{2y} are the normal components of the wavevector in vacuum and the antiferromagnet respectively, and are given by

$$k_{1y} = \sqrt{k_0^2 - k_x^2} \tag{17}$$

and

$$k_{2y} = \sqrt{\epsilon\mu_v k_0^2 - k_x^2}. \tag{18}$$

Since $k_x(\theta_1) = -k_x(-\theta_1)$ and $\mu_2(\mathbf{B}_0) = -\mu_2(-\mathbf{B}_0)$, the effect of either changing the sign of θ_1 or changing the sign of B_0 is to change the sign of the term $ik_x(\mu_2/\mu_1)$ in both the numerator and the denominator of Equation 14, all other terms in this equation being unaffected.

Let us first consider how this sign change affects the complex reflection coefficient r in the case of zero absorption ($\Gamma = 0$). In this case, all the parameters in Equation 14 are real, except for k_{2y}, which may be either real or imaginary depending on the frequency. When k_{2y} is real, there is propagation of radiation, as bulk polaritons, into the interior of the sample. When it is imaginary the field within the antiferromagnet is evanescent, decaying away from the interface. We refer to frequencies corresponding to k_{2y} real as bulk region frequencies and those corresponding to k_{2y} imaginary as reststrahl region frequencies.

At bulk region frequencies (k_{2y} real), separation of Equation 14 into real and imaginary parts leads to

$$r^*(\mathbf{B}_0) = r(-\mathbf{B}_0). \tag{19}$$

The overall reflectivity is given by

$$R = rr^*, \tag{20}$$

and is therefore reciprocal.

At reststrahl region frequencies (k_{2y} imaginary), the numerator of Equation 14 is the complex conjugate of the denominator. Thus one can see from Equation 20 that R must be equal to 1, regardless of the sign of B_0, so once again the reflectivity is reciprocal. The result $R = 1$ is of course what one should expect, since when k_{2y} is imaginary there is no propagation into the sample, leading to total reflection.

Simulated oblique incidence ($\theta_1 = 45°$) reflectivity spectra off MnF_2 at 4.2 K, in an external magnetic field $\mathbf{B}_0$ of magnitude 0.1 T, are shown in Figure 2(a), in which zero damping is assumed. The frequency scale is expressed in terms of wavenumbers $\omega/2\pi c$, and the MnF_2 parameters used in the calculation are (Dumelow & Oliveros, 1997) ϵ =5.5, M_S =6.0×10^5 A/m,

B_A = 0.787 T, B_E = 53.0 T and γ = 0.975 cm^{-1}/T, corresponding to ω_r = 8.94 cm^{-1}. The curves for B_0 = +0.1 T and B_0 = −0.1 T are coincident at all frequencies, confirming that the reflectivity is reciprocal.

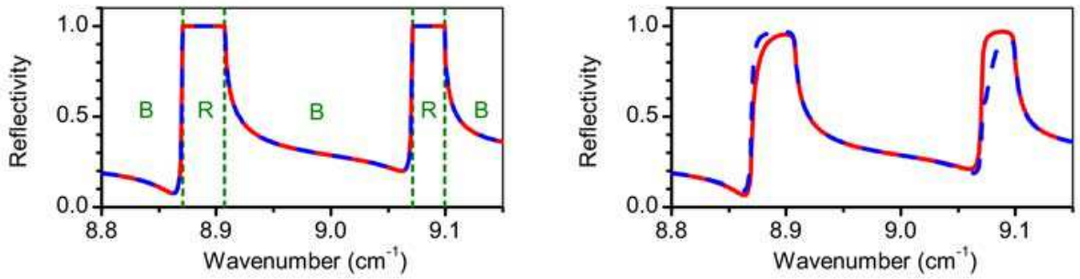

(a) Ignoring damping (b) Damping included

Fig. 2. Calculated oblique incidence (θ_1 = 45°) reflectivity spectrum off MnF_2 in an external field of B_0 = +0.1 T (solid curves) and B_0 = −0.1 T (dashed curves). Note that in (a) the two curves are coincident. The symbols B and R in (a) represent the bulk and reststrahl frequency regions respectively.

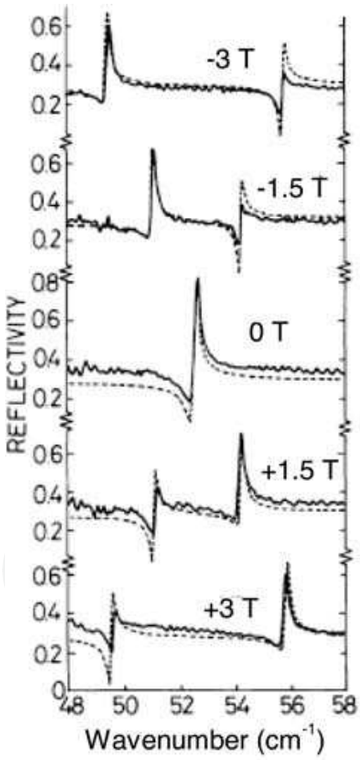

Fig. 3. Experimental (solid curves) and theoretical (dashed curves) oblique incidence reflectivity (θ_1 = 45°) reflectivity spectra off FeF_2 at 4.2 K, in the presence of positive and negative external magnetic fields. After Brown et al. (1994).

When the damping is nonzero, the above symmetry arguments do not apply, and the reflectivity R is, in general, nonreciprocal. This can be seen from Figure 2(b), in which damping has been included in the calculation, using the experimental value of Γ = 0.0007

cm^{-1}. In this figure, the curves for B_0 = +0.1 T and B_0 = −0.1 T are not coincident. The difference in this case is quite small, since the damping in MnF_2 is small. Remer et al. (1986) was able to observe this small difference experimentally using a field scan at fixed frequency, but found a larger nonreciprocity at higher temperature, corresponding to larger damping. 4.2 K frequency scans of the type shown in Figure 2 have been performed on FeF_2 (Brown et al., 1994), which has a considerably higher damping parameter than MnF_2, using far infrared Fourier transform spectroscopy (Brown et al., 1998). In this case the nonreciprocity in the reflectivity is quite clear, as seen in Figure 3.

3.2 Reflected phase

The complex reflection coefficient r given by Equation 14 is commonly expressed in terms of a reflection amplitude ρ_r and phase ϕ_r:

$$r = \rho_r \exp(i\phi_r), \tag{21}$$

where

$$\rho_r = R^{1/2}, \tag{22}$$

and

$$\phi_r = \tan^{-1}\left[\frac{\mathrm{Im}(r)}{\mathrm{Re}(r)}\right]. \tag{23}$$

Although thermodynamic arguments show that, in the absence of damping, the reflected intensity R, and hence the amplitude ρ_r, should be reciprocal (Remer et al., 1984), such arguments cannot be applied to the reflected phase ϕ_r. A detailed discussion of nonreciprocity in the reflected phase on reflection off antiferromagnets is given in Dumelow et al. (1998). Here we summarise the main results.

We consider first the case of zero damping (Γ = 0). In the bulk regions, Equation 19 should apply. Thus, since the phase is given by Equation 23, we can see quite straightforwardly that

$$\phi_r(\mathbf{B}_0) = -\phi_r(-\mathbf{B}_0) + 2\pi m, \tag{24}$$

where m is an arbitrary integer. We include the term $2\pi m$ since it is convenient to plot the phase outside the range $-\pi < \phi_r < \pi$.

Equation 24 shows that, in the bulk regions, the reflected phase is nonreciprocal even in the absence of damping. This is also the case in the reststrahl regions, but the phase does not follow a simple symmetry relation of the type given by this equation.

The amplitude and phase for reflection off MnF_2 in the absence of damping are shown in Figures 4(a) and 4(c) respectively. The conditions are the same as those used in Figure 2. Note that we have shown the phase as varying within the range π to 3π in order to show that it changes continuously with frequency. The amplitude is reciprocal, in agreement with Figure 2, but nonreciprocity in the reflected phase is quite marked in both the bulk and reststrahl regions, obeying Equation 24 in the bulk regions.

Figures 4(b) and 4(d) show reflection amplitude and phase respectively in the presence of damping. In line with the reflectivity results in the previous subsection, the reflection amplitude now shows slight nonreciprocity. The phase shows the same type of nonreciprocity as seen without damping, although the bulk region symmetry arguments of Equation 24 no longer apply.

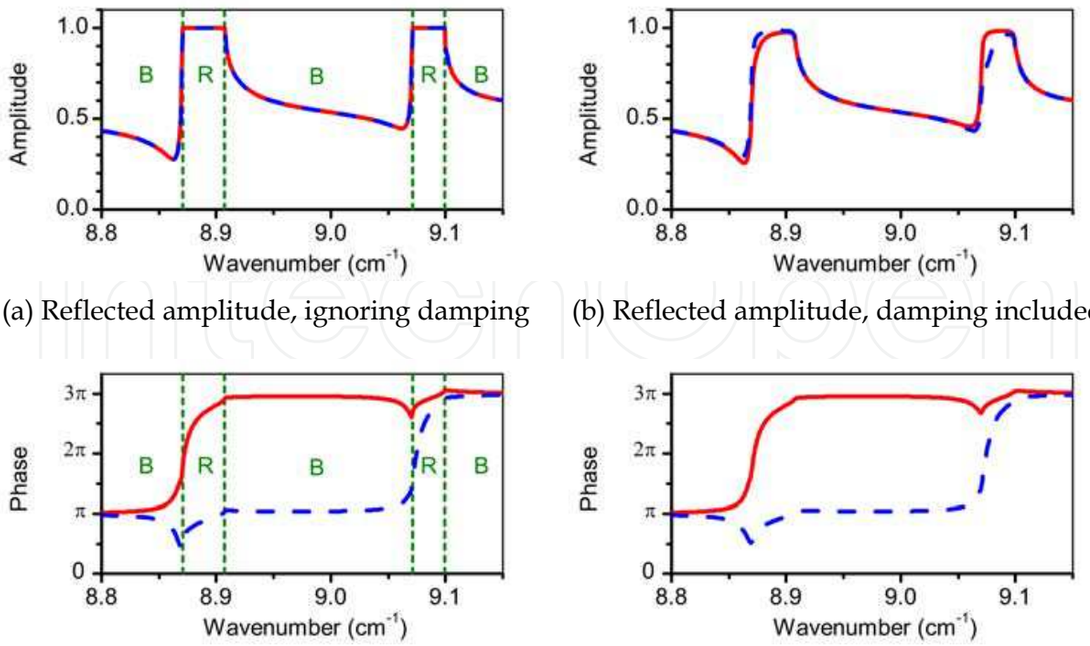

(a) Reflected amplitude, ignoring damping (b) Reflected amplitude, damping included

(c) Reflected phase, ignoring damping (d) Reflected phase, damping included

Fig. 4. Calculated reflected amplitude and phase spectra for oblique incidence (θ=45°) reflection off MnF_2 in an external field of $B_0 = +0.1$ T (solid curves) and $B_0 = -0.1$ T (dashed curves). Note that in (a) the two curves are coincident. The symbols B and R represent the bulk and reststrahl frequency regions respectively.

3.3 Power flow

The nonreciprocal phenomena described in the Subsections 3.1 and 3.2 were analysed ten or more years ago, and concern the behaviour of a reflected plane wave. Recently we have started studying nonreciprocal behaviour within the antiferromagnet itself, in particular with respect to the direction of the internal power flow (Lima et al., 2009), represented by the time-averaged Poynting vector (Landau & Lifshitz, 1984),

$$\langle \mathbf{S} \rangle = 1/2 \ \mathrm{Re}\left(\mathbf{E} \times \mathbf{H}^* \right). \tag{25}$$

We consider an angle of refraction in terms of the direction of the time-averaged Poynting vector $\langle \mathbf{S}_2 \rangle$ (which is not necessarily the same as the wavevector direction) in the antiferromagnet, as shown in Figure 5. The angle of refraction θ_2, defined in this way, is given by

$$\tan\theta_2 = \frac{\langle S_{2x} \rangle}{\langle S_{2z} \rangle}. \tag{26}$$

In s polarisation the **E** field is confined along z, so the Poynting vector is most easily represented in terms of the E_z field, making use of the conversion $\mathbf{k} \times \mathbf{E} = \omega\mu_0\boldsymbol{\mu}\mathbf{H}$. The resulting time averaged Poynting vector has components

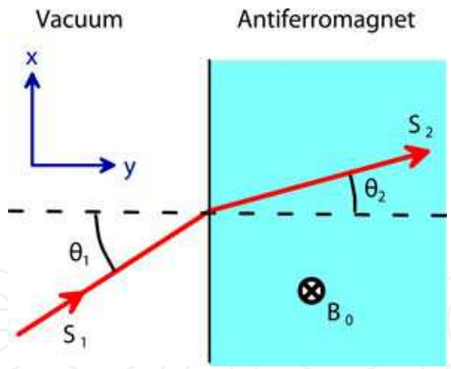

Fig. 5. Angle of refraction θ_2 defined by power flow direction.

$$\langle S_{2x} \rangle = \frac{|E_z|^2}{2\omega\mu_0} \operatorname{Re}\left[\frac{k_x - ik_{2y}(\mu_2/\mu_1)}{\mu_v}\right], \tag{27}$$

$$\langle S_{2y} \rangle = \frac{|E_z|^2}{2\omega\mu_0} \operatorname{Re}\left[\frac{k_{2y} + ik_x(\mu_2/\mu_1)}{\mu_v}\right]. \tag{28}$$

The direction of power flow can thus be obtained by substitution into Equation 26.
We now investigate the above expressions in order to search for possible nonreciprocity in the power flow direction in the antiferromagnet, taking power flow to be nonreciprocal if

$$\theta_2(-\mathbf{B}_0) \neq \theta_2(\mathbf{B}_0). \tag{29}$$

In order to consider power flow, we restrict ourselves initially to the case where there is no damping in the system ($\Gamma = 0$). The calculated values of θ_2 for oblique incident reflection off MnF_2 in this case are shown in Figure 6.

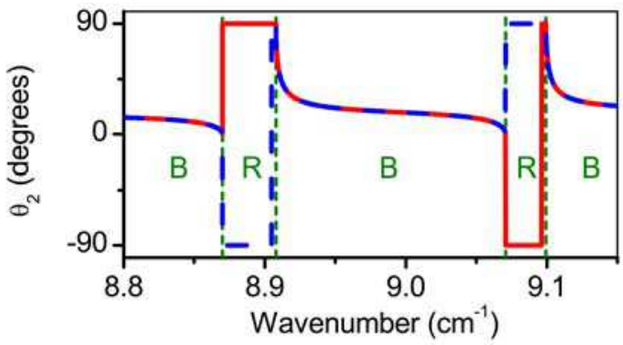

Fig. 6. Calculated θ_2 values on oblique incidence reflection ($\theta_1 = 45°$) off MnF_2 in a field of B_0 = +0.1 T (solid curve) and B_0 = −0.1 T (dashed curve), ignoring damping. Both curves are coincident in the bulk regions. The symbols B and R represent the bulk and reststrahl frequency regions (separated by dashed vertical lines) respectively.

In the case of zero damping, as discussed previously, μ_1, μ_2, and μ_v are all wholly real. k_{2y} is real in the bulk regions and imaginary in the reststrahl regions.
First we consider power flow for k_{2y} real (i.e. in the bulk regions). Equations 27 and 28 then give

$$\langle S_{2x} \rangle = \frac{|E_z|^2 k_x}{2\omega\mu_0\mu_v}, \tag{30}$$

$$\langle S_{2y} \rangle = \frac{|E_z|^2 k_{2y}}{2\omega\mu_0\mu_v}, \tag{31}$$

Thus, since none of the terms in Equations 30 and 31 depend on the sign of B_0, we see that the power flow direction is reciprocal ($\theta_2(-B_0) = \theta_2(B_0)$). We also see from Equations 26, 30 and 31 that

$$\tan\theta_2 = \frac{k_x}{k_{2y}}, \tag{32}$$

so that $\mathbf{S}_2$ is parallel to $\mathbf{k}_2$. Since k_x is continuous and k_{2y} positive it also follows that refraction must be positive, i.e. θ_2 always has the same sign as θ_1. Overall, therefore, power flow follows the type of behavior shown in Fig. 7(a). This is confirmed by the calculations of the θ_2 shown in Figure 6 for the bulk regions. Note that in these regions radiation may, in principle, flow an infinite distance into the antiferromagnet, and is thus unaffected by the sample surface. Our result that power flow is reciprocal in this case is thus consistent with the idea that radiation should display reciprocal behavior in the interior of a sample.

(a) Bulk regions (b) Lower reststrahl region

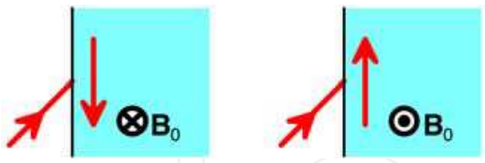

(c) Upper reststrahl region

Fig. 7. Power flow in the various spectral regions for oblique incidence radiation.

We now consider the case when k_{2y} is imaginary. In this case we get

$$\langle S_{2x} \rangle = \frac{|E_z|^2 \left[k_x - ik_{2y}(\mu_2 / \mu_1) \right]}{2\omega\mu_0\mu_v}, \tag{33}$$

$$\langle S_{2y} \rangle = 0. \tag{34}$$

There is thus no propagation into the antiferromagnet, but energy can travel along the surface in the form of an evanescent wave within the antiferromagnet. In such cases, which are characterized by $\theta_2 = \pm 90°$, the angle θ_2 does not describe refraction in the normal sense of the word, since the associated radiation has an evanescent component. Indeed there is no

transfer of radiation across the interface, since power is wholly reflected. The direction of power flow may or may not be reciprocal, depending on the relative magnitudes of the two terms in the numerator of Equation 33. However, if the external field is sufficiently large, the second term dominates within both reststrahl regions. In the present example, for $B_0 = \pm 0.1$ T, this results in $\theta_2 = \pm 90°$ in most of the lower reststrahl region (Figure 7(b)) and $\theta_2 = \mp 90°$ in most of the upper reststrahl region (Figure 7(c)), as shown in the calculation in Figure 6, and nonreciprocity, as defined by Equation 29, occurs. There is, however, a narrow region of reciprocal power flow (in terms of direction if not of magnitude) near the upper frequency limit of each reststrahl region.

Possibly one of the most interesting aspects of the power flow is its behaviour in the case of normally incident radiation (Lima et al., 2009). The calculated θ_2 values are shown in Figure 8. In the bulk regions, as expected, power flow is normal to the surface, as shown in Figure 9(a). In the reststrahl regions, however, power flow parallel to the sample surface is induced in the same way as occurs at oblique incidence. The direction of this power flow depends on the sign of the external field, as shown in Figures 9(b) and 9(c). This is distinctly counter-intuitive considering that we are modelling plane waves normally incident on an infinite surface, so that there should be no spatial variation of the field along x. Nevertheless, the

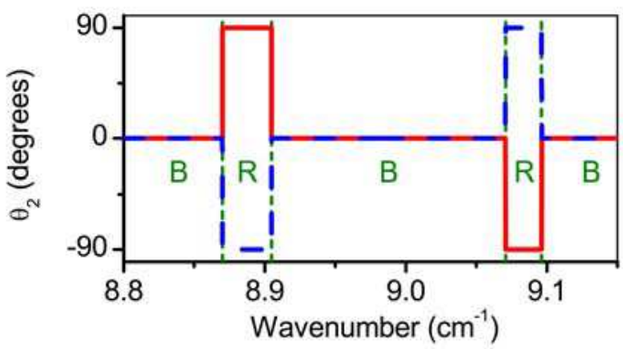

Fig. 8. Calculated θ_2 values on normal incidence reflection off MnF_2 in a field of $B_0 = +0.1$ T (solid curve) and $B_0 = -0.1$ T (dashed curve), ignoring damping. The symbols B and R represent the bulk and reststrahl frequency regions (separated by dashed vertical lines) respectively. After Lima et al. (2009).

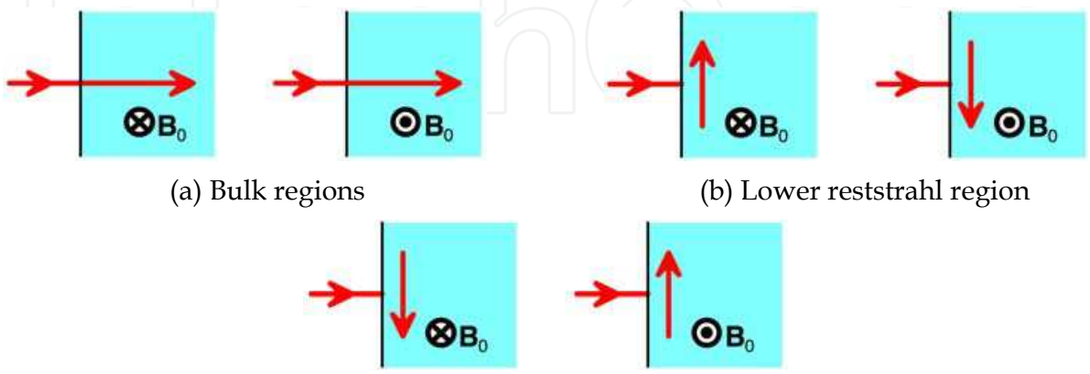

(a) Bulk regions (b) Lower reststrahl region

(c) Upper reststrahl region

Fig. 9. Power flow in the various spectral regions for normal incidence radiation.

very fact that the field is assumed to extend over an infinite plane means that energy flow along the surface does not violate causality.

We now turn to the case where damping is present. Now k_{2y} should, in general, be complex, with the its imaginary part greater near the reststrahl regions. Since imaginary k_{2y} results in nonreciprocal power flow, we should also expect such nonreciprocity in the case of complex k_{2y}. In Fig. 10 we show the power flow directions both for normal and for oblique incidence, assuming $\Gamma = 0.0007\text{cm}^{-1}$. There is now no distinct division between reststrahl and bulk regions, and nonreciprocal power flow occurs both inside and outside the nominal reststrahl regions. At normal incidence the power flow directions are now no longer restricted to $\theta_2 = 0°$ and $\theta_2 = \pm 90°$. Since nonzero θ_2 implies nonreciprocity, the associated fields must be some extent be bound to the sample surface in all regions for which $\theta_2 \neq 0°$.

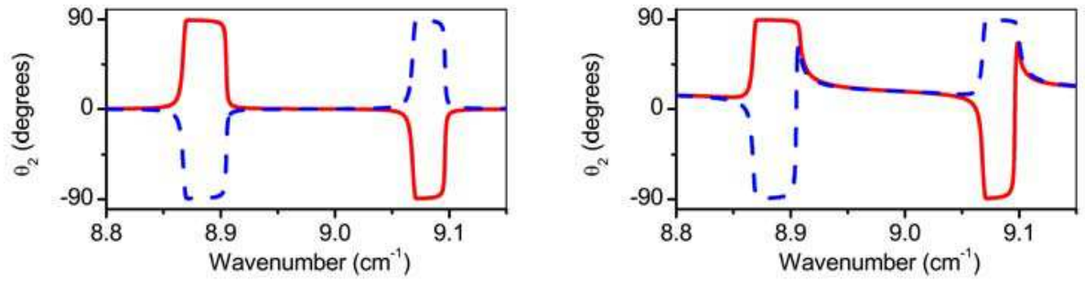

(a) $\theta_1 = 0$ (b) $\theta_1 = 45°$

Fig. 10. Calculated θ_2 values on reflection off MnF_2 in a field of $B_0 = +0.1$ T (solid curve) and $B_0 = -0.1$ T (dashed curve), assuming a damping parameter of $\Gamma = 0.0007$ cm^{-1}.

4. Reflection of a finite beam

4.1 Introduction

The previous section discusses various phenomena associated with plane wave reflection off an antiferromagnet. However, when the plane wave is replaced by a finite beam, we predict additional effects concerning the profile and position of the reflected beam (Lima et al., 2008; 2009). Such effects are expected with either normal or oblique incidence radiation. However, we concentrate on normal incidence effects firstly for simplicity and secondly because they are more unexpected.

We examine reflection of finite beams in two ways. Firstly, we interpret the reflection using an angular spectrum analysis, in which the incident beam is considered as a Fourier sum of plane waves. We then give a power flow interpretation of the predicted effects.

4.2 Angular spectrum analysis

Here we summarise the angular spectrum analysis used in describing reflection of a finite beam normally incident on an antiferromagnet (Lima et al., 2008), using a two dimensional model in which the incident beam, centred at $x = 0$, is considered as an angular spectrum of plane waves propagating in the xy plane. It can thus be represented in the form

$$E_i(x,y) = \int_{-k_0}^{k_0} \psi(k_x) \exp\left[i\left(k_x x + k_{1y} y\right)\right] dk_x, \tag{35}$$

where $\psi(k_x)$ is a distribution function representing the shape of the beam. At the sample surface, which we place at $y = 0$, the electric field of the incident beam is

$$E_i(x,0) = \int_{-k_0}^{k_0} \psi(k_x) \exp\left(ik_x x\right) dk_x. \tag{36}$$

The electric field of the corresponding reflected beam is given, at the surface, by

$$E_r(x,0) = \int_{-k_0}^{k_0} r(k_x)\psi(k_x) \exp\left(ik_x x\right) dk_x. \tag{37}$$

Here $r(k_x)$ represents the complex reflection coefficient for the relevant plane wave component, and is given by Equation 14. It is convenient to consider this complex coefficient in terms of amplitude $\rho_r(k_x)$ and phase $\phi_r(k_x)$, in the form of Equation 21, i.e.,

$$r(k_x) = \rho_r(k_x) \exp\left[i\phi_r(k_x)\right]. \tag{38}$$

If the beam is sufficiently wide, there will be a narrow distribution of k_x values centred, at normal incidence, around $k_x = 0$. We can thus substitute Equation 38 into Equation 37 and expand $\rho_r(k_x)$ and $\phi_r(k_x)$ as a Taylor series around $k_x = 0$. If we ignore terms in k_x^2 and above, this leads to

$$E_r(x,0) = r(0)\int_{-k_0}^{k_0} \psi(k_x) \exp\left(ik_x X\right) dk_x + r'(0)\int_{-k_0}^{k_0} k_x\psi(k_x) \exp\left(ik_x X\right) dk_x, \tag{39}$$

where

$$r(0) = \rho_r(0) \exp\left[i\phi_r(0)\right], \tag{40}$$

$$r'(0) = \frac{d\rho_r}{dk_x}\Big|_{k_x=0} \exp\left[i\phi_r(0)\right], \tag{41}$$

$$X = x + \frac{d\phi_r}{dk_x}\Big|_{k_x=0}. \tag{42}$$

The second term on the right hand side of Equation 39 can, in practice, normally be ignored (Lima et al., 2008). In fact, in the absence of damping, it is identically zero since reciprocity in ρ_r implies $d\rho_r / dk_x|_{k_x=0} = 0$, and hence $r'(0) = 0$. Even in the presence of damping, however, the contribution of this term is negligible for a sufficiently narrow k_x distribution.
The reflected field is thus given, to a good approximation, by the first term on the right hand side of Equation 39. This term is simply the reflection coefficient $r(0)$ for a normally incident plane wave multiplied by an integral which gives the profile of the field along x. This integral is identical to that of the incident beam (Equation 36) except that x has been replaced by X, given by Equation 42. Thus the shape of the reflected beam is the same as that of the incident beam, but it has been shifted along the surface of the sample by a distance D_r equal to

$$D_r = -\frac{d\phi_r}{dk_x}\Big|_{k_x=0} \tag{43}$$

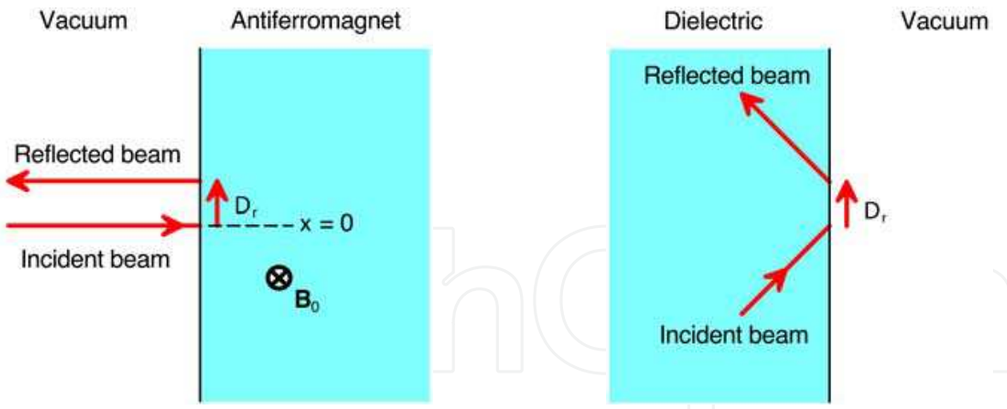

(a) Normal incidence reflection off AF (b) Conventional Goos-Hänchen shift

Fig. 11. Comparison of the normal incidence Goos-Hänchen shift predicted for external reflection off an antiferromagnet with the conventional Goos Hänchen shift for total internal reflection.

as shown in Figure 11(a). In the case of reciprocal reflected phase (i.e. $\phi(-k_x) = \phi(k_x)$), $d\phi_r / dk_x |_{k_x=0}$ must be zero, so there will be no lateral shift. In the case of reflection off antiferromagnets, however, the reflected phase is, in general, nonreciprocal, as discussed in Section 3.2, and a nonzero displacement of the reflected beam is expected.

Before discussing the lateral shift described by Equation 43 in any detail, we note that the behaviour of the reflected beam is in some ways similar to that of an oblique incidence finite beam which undergoes total internal reflection when passing from an optically denser to a less dense medium. Such a beam also suffers a lateral displacement D_r upon reflection, as shown in Figure 11(b). This displacement was observed experimentally by Goos & Hänchen (1947) and is normally referred to as a Goos-Hänchen shift (Lotsch, 1970). Goos-Hänchen shifts have also been reported in the case of external reflection in specific instances such as reflection off metals (Wild & Giles, 1982; Leung et al., 2007), and the lateral displacement discussed here can be considered as a type of a normal incidence Goos-Hänchen shift. Equation 43 is, indeed, a normal incidence version of the classical expression commonly used to describe Goos-Hänchen shifts (Artmann, 1948), and the angular spectrum analysis used above in deriving the equation is basically the same as that previously used to describe Goos-Hänchen shifts in the case of total internal reflection (Horowitz & Tamir, 1971; McGuirk & Carniglia, 1977).

We now apply Equation 43 to the specific case of reflection off an antiferromagnet. In the absence of damping, the reflection coefficient r can easily be resolved into its real and imaginary parts, allowing explicit evaluation of this equation. This gives

$$D_r = \frac{2(\mu_2/\mu_1)}{k_0(\mu_v - \epsilon)} \tag{44}$$

in both the bulk and the reststrahl regions. Since the sign of μ_2 depends on the sign of B_0, it is immediately obvious that the direction of the lateral displacement will be reversed if the external field direction is reversed. In the presence of damping, Equation 43 can be evaluated numerically, but the results are found to be almost identical to those with $\Gamma = 0$ (Lima et al., 2008).

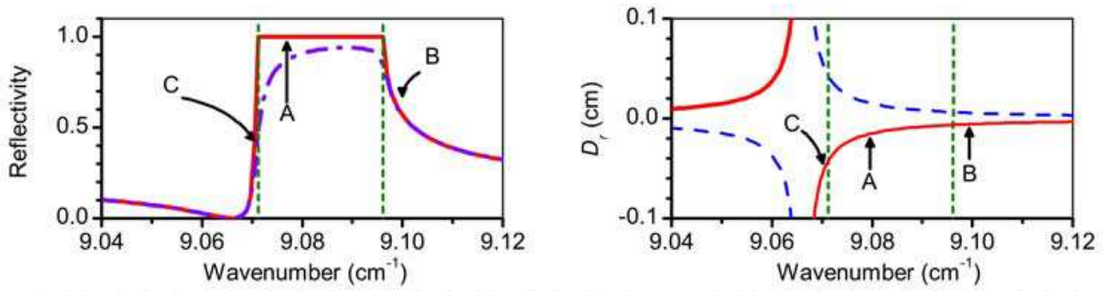

(a) Reflectivity (b) Lateral shift of reflected beam

Fig. 12. Calculated normal incidence reflectivity spectrum and 1ateral shift for reflection off MnF_2 in an external field of $B_0 = +0.1$ T. In (a) the solid curve is calculated without damping and the dot-dash curve with $\Gamma = 0.0007$ cm^{-1}. In (b) the solid curves are for an external field of $B_0 = \pm 0.1$ T and the dashed curves for an external field of $B_0 = -0.1$ T. The vertical lines separate the bulk and reststrahl regions. The marked frequencies are A: 9.0769 cm^{-1}; B: 9.0994 cm^{-1}; C: 9.0705 cm^{-1}. After Lima et al. (2009).

The calculated values of D_r, ignoring damping, are compared with the reflectivity spectrum at upper reststrahl region frequencies in Figure 12. A lateral shift is predicted in both the bulk and the reststrahl regions. Similar shifts are predicted around the lower reststrahl region, but of opposite sign (Lima et al., 2008). There is a divergence in D_r at the reflectivity minimum just below the reststrahl region. At this frequency, the assumptions made in deriving Equation D_r clearly do not apply.

In order ot verify the shifts shown in Figure 12, reflection of a particular incident beam profile may be modelled. For simplicity, we have considered a gaussian beam whose focal plane is the surface of the sample (Lima et al., 2008; 2009). The incident beam can thus be represented by Equation (35) with (Horowitz & Tamir, 1971)

$$\psi(k_x) = \frac{g}{2\sqrt{\pi}} \exp\left(-\frac{g^2 k_x^2}{4}\right), \tag{45}$$

where $2g$ represents the beam width at the focal plane. At the sample surface the incident beam profile is thus represented by Equation 36 and the reflected beam profile by Equation 37. The integrals in these two equations can be evaluated numerically, and the profiles of the corresponding **E** fields thus obtained.

The incident and reflected beam intensities can, in general, be well represented by $|E|^2$. In Figure 13 we show the resulting intensity profiles along x for the three frequencies marked in Figure 12. It is seen that, although the modelled incident beam is very narrow ($g = \lambda$, the free space wavelength), all the reflected beams are displaced along the surface in excellent agreement with Equation 44. It is also observed that damping does not noticeably affect this displacement. Explicit simulations have also confirmed the prediction of Equation 44 that beam displacement is, to a very good approximation, independent of beam width (Lima et al., 2008).

It is useful not only to consider the incident and reflected fields at the surface, but also the overall **E** field distribution in the xy plane. We conveniently consider the electric fields in terms of an incident field $E_i(x,y)$ and a reflected field $E_r(x,y)$ in the region $x < 0$ (vacuum) and a transmitted field $E_t(x,y)$ in the region $x > 0$ (antiferromagnet). $E_i(x,y)$ is given by Equation 35, with $E_r(x,y)$ and $E_t(x,y)$ given by

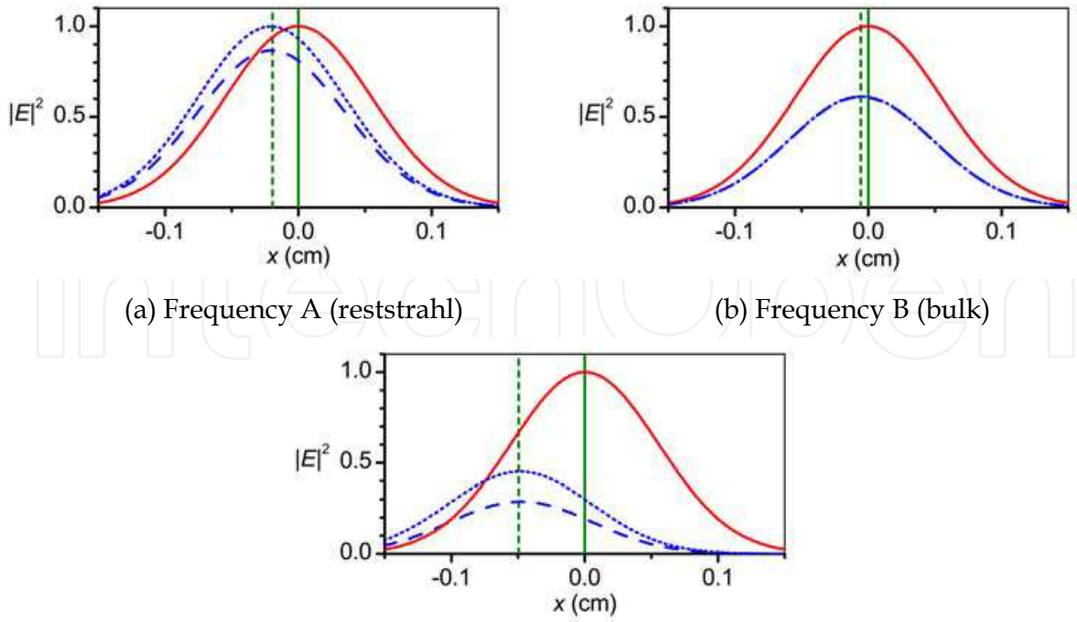

(a) Frequency A (reststrahl) (b) Frequency B (bulk)

(c) Frequency C (bulk)

Fig. 13. Intensity profiles, along the sample surface, in the case of reflection of a normally incident gaussian beam off MnF_2 in an external magnetic field of 0.1 T. Solid curve: incident beam; dotted curve: reflected beam ignoring damping; dashed curve: reflected beam with $\Gamma = 0.0007$ cm^{-1}; vertical solid line: centre of incident beam; vertical dashed line: centre of reflected beam predicted by Equation 44. Note that, in (b), the reflected intensities with and without damping are almost identical, and the curves cannot be separated. After Lima et al. (2009).

$$E_r(x,y) = \int_{-k_0}^{k_0} r(k_x)\psi(k_x)\exp\left[i\left(k_x x - k_{1y} y\right)\right]dk_x \tag{46}$$

and

$$E_t(x,y) = \int_{-k_0}^{k_0} t(k_x)\psi(k_x)\exp\left[i\left(k_x x + k_{2y} y\right)\right]dk_x \tag{47}$$

respectively. The resulting profiles at the three frequencies indicated in Figure 12 are shown in Figures 14 and 15. Figure 14 shows the profile in the absence of damping and Figure 15 shows the profile when damping is included. The left hand panels show the incident and transmitted fields, whilst the right hand panels show the reflected field.

In all cases the reflected fields are displaced along x in accordance with Figures 12 and 13. In addition, we see that the transmitted field is also displaced. This result can be anticipated from the fact that the phase ϕ_t of the complex transmission coefficient t is nonreciprocal. An analysis equivalent to that used in determining D_r then gives a lateral displacement D_t of the transmitted field profile given by

$$D_t = -\frac{d\phi_t}{dk_x}\Big|_{k_x=0}. \tag{48}$$

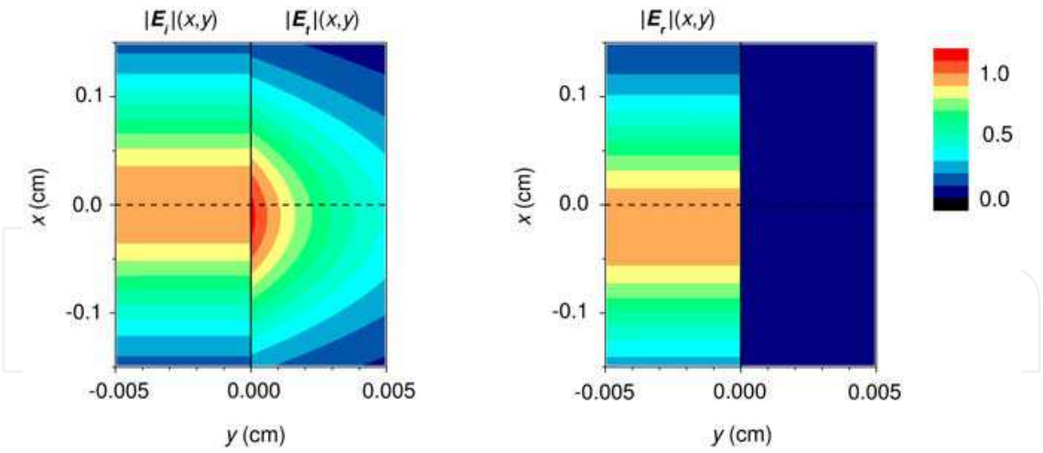

(a) Frequency A (reststrahl)

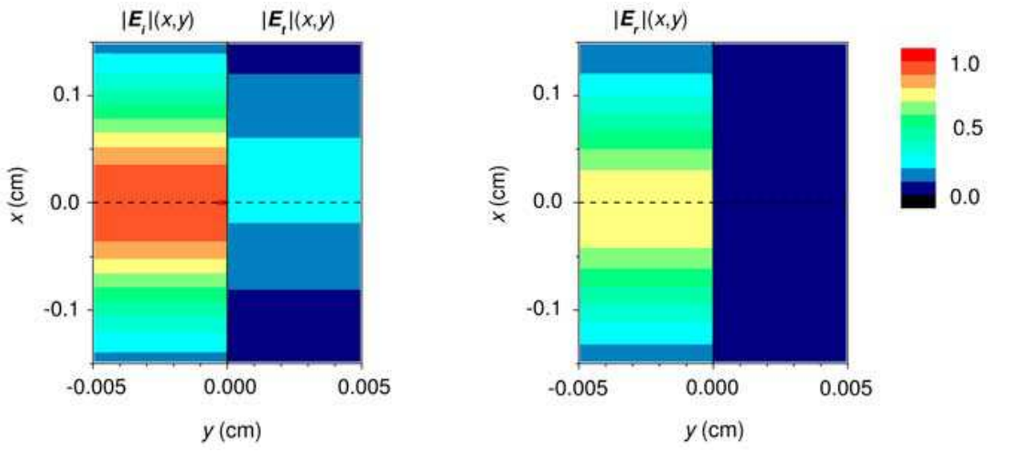

b) Frequency B (bulk)

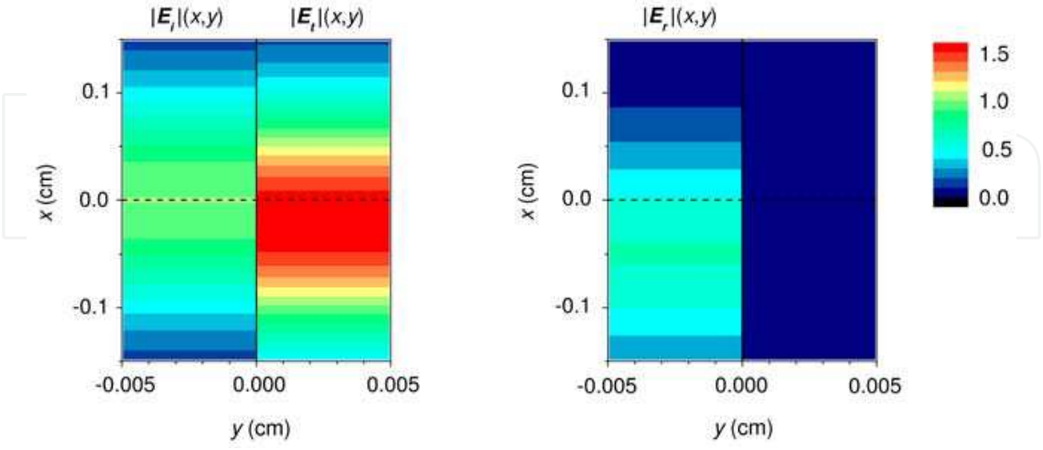

(c) Frequency C (bulk)

Fig. 14. Profiles of the amplitudes of the incident ($E_i(x,y)$), transmitted ($E_t(x,y)$), and reflected ($E_r(x,y)$) fields in the case of reflection of a normally incident gaussian beam off MnF_2 in an external magnetic field of 0.1 T, ignoring damping. After Lima et al. (2009).

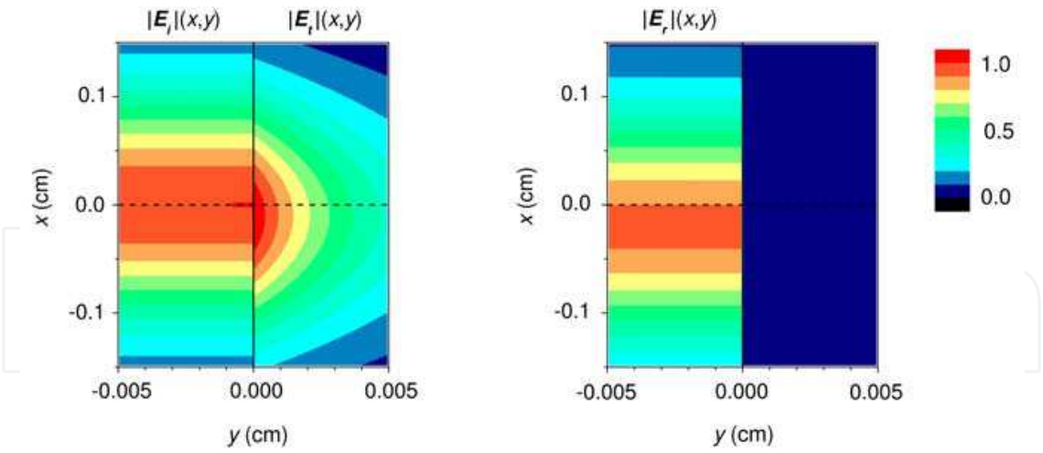

(a) Frequency A (reststrahl)

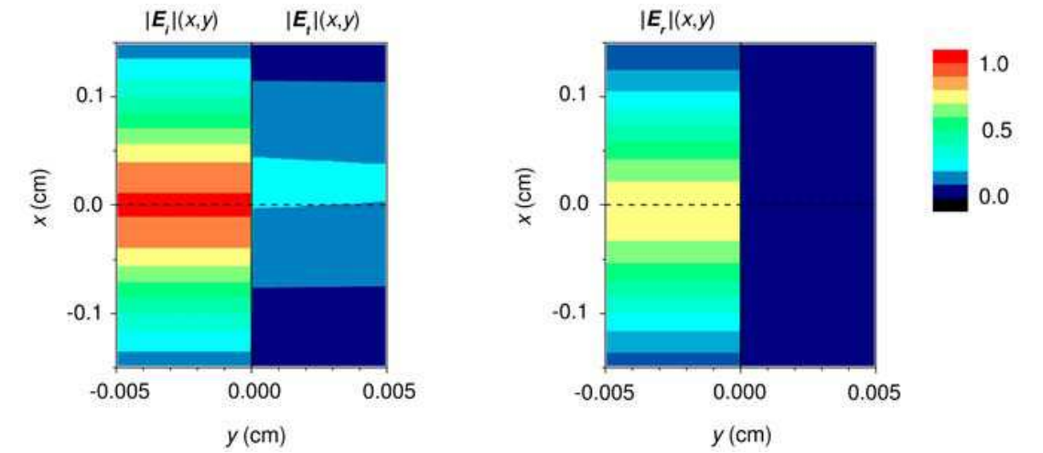

(b) Frequency B (bulk)

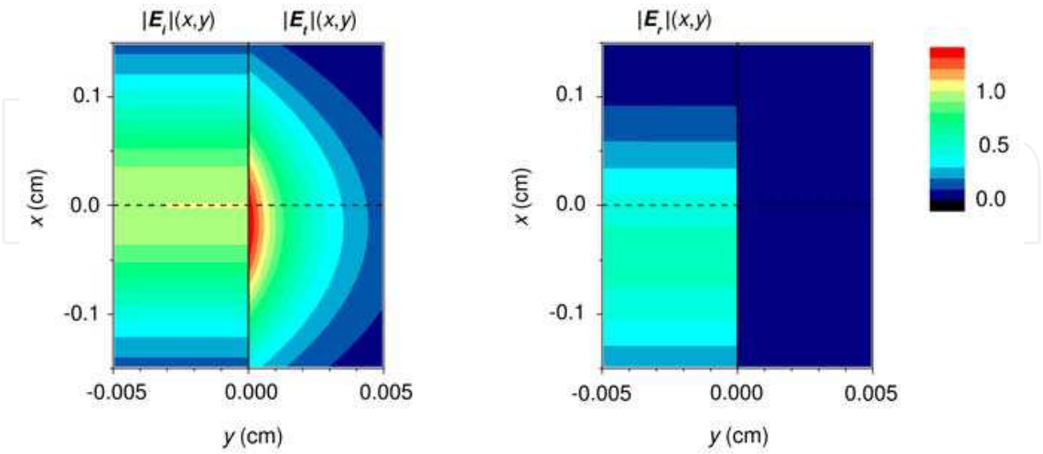

(c) Frequency C (bulk)

Fig. 15. Profiles of the amplitudes of the incident ($E_i(x,y)$), transmitted ($E_t(x,y)$), and reflected ($E_r(x,y)$) fields in the case of reflection of a normally incident gaussian beam off MnF_2 in an external magnetic field of 0.1 T, for $\Gamma = 0.0007$ cm^{-1}.

It is noticeable that, in the case of the bulk frequency B, near the top of the reststrahl band, there is a much larger displacement in the transmitted field than in that of the reflected beam. In the absence of damping, the field decays away from the interface in the reststrahl region (Figure 14(a)), but propagates into the sample, perpendicular to the surface, in the bulk regions (Figures 14(b) and 14(c)). When damping is included, the reststrahl region behaviour is largely unchanged, but there may now be significant decay in the bulk regions. At frequency B, just above the top of the reststrahl region, this decay is fairly small, but at frequency C, near the bottom of the reststrahl region, it is similar to that in the reststrahl region itself.

4.3 Power flow analysis

4.3.1 Reststrahl region

In the above analysis we have considered the displacement of the reflected beam as an interference effect. It is also useful, however, to consider this effect in terms of power flow. In the reststrahl regions, in the absence of absorption, energy conservation principles can be used in a straightforward way to analyse the lateral shift (Lima et al., 2009). The analysis is similar to that used by Renard (1964) in the case of the conventional Goos-Hänchen shift for total internal reflection.

We make use of the result of subsection 3.3 that, in the reststrahl regions and in the absence of damping, a normally incident plane wave reflected off an antiferromagnet induces power flow parallel to the surface within the antiferromagnet, as shown in Figures 9(b) and 9(c). We consider this to be the behaviour in the centre portion of a wide finite incident beam, such as that represented in Figure 16. The central portion of this incident beam lies between x_2 and x_3, and it gradually decays away to zero between x_2 and x_1 and between x_3 and x_4. The internal energy flux associated with plane wave reflection in the central portion is represented by P_2. Energy conservation therefore requires that there is a net flux P_1 entering the antiferromagnet near one edge of the beam and a net flux leaving near the other edge. This is equivalent to a lateral shift D_r of the reflected beam with respect to the incident beam. Thus P_1 enters in the region between x_1 and $x_2 + D_r$ and P_3 leaves in the region between x_3 and $x_4 + D_r$. We consider energy flow within a slice, of thickness Δz, in the xy plane. Within this slice we have $P_1 = P_2 = P_3$.

P_1 is the difference between the incident and reflected flux between X_2 and $x_2 + D_r$, and can be written as

$$P_1 = \int_{x_1}^{x_2} \langle S_i(x) \rangle \Delta z \, dx + \int_{x_2}^{x_2+D_r} \langle S_i(x) \rangle \Delta z \, dx + \int_{x_1+D_r}^{x_2+D_r} \langle S_r(x) \rangle \Delta z \, dx, \tag{49}$$

where $\langle S_i(x) \rangle$ and $\langle S_r(x) \rangle$ are the intensities, represented in terms of time averaged Poynting vectors along y, of the incident and reflected waves respectively. Since we expect the reflected beam to have the same shape as the incident beam, we can write

$$\langle S_i(x) \rangle = -\langle S_r(x + D_r) \rangle, \tag{50}$$

so that the first and last terms on the right hand side of Equation 49 cancel. Thus only the second term contributes to P_1, and the integral is only performed between x_2 and $x_2 + D_r$, in the central portion of the beam. Within this interval $\langle S_i(x) \rangle$ has a constant value, which we denote as $\langle S_{\max} \rangle$. Equation 49 thus becomes

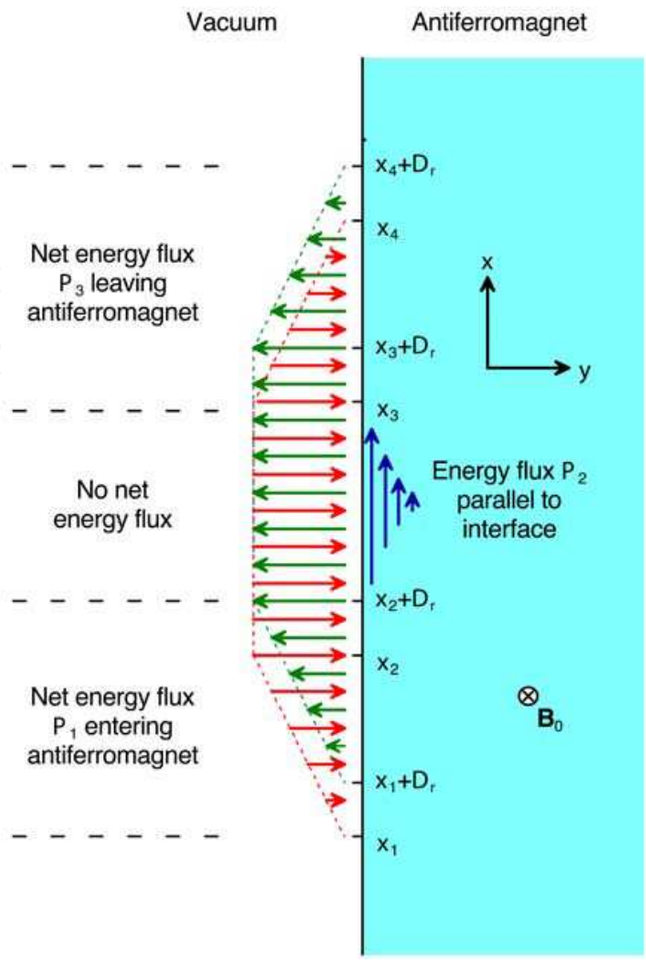

Fig. 16. Model of lateral displacement of reflected beam in the reststrahl regions in terms of power flow along the antiferromagnet surface.

$$P_1 = \langle S_{max} \rangle \Delta z D_r . \tag{51}$$

Using Equation 25 and a standard application of Maxwell's equations, $\langle S_{\max} \rangle$ can be expressed in terms of the incident field $E_{\max}$ within the central region of the beam as

$$\langle S_{max} \rangle = \frac{k_0 \left| E_{max} \right|^2}{2\omega\mu_0}. \tag{52}$$

The flux P_2 within the antiferromagnet is given by

$$P_2 = \int_0^\infty \langle S_{2x}(y) \rangle \Delta z \, dy. \tag{53}$$

$\langle S_{2x}(y) \rangle$ can be expressed in terms of the electric field $E_z(y)$ within the antiferromagnet using Equation 27. $E_z(y)$ itself can be related to the field $E_{\max}$ of the incident beam by the equation

$$E_z(y) = tE_{max} \exp\left(ik_{2y} y\right), \tag{54}$$

so P_2 may also be obtained as a function of E_{max}. On putting $P_1 = P_2$ in the above equations, and solving for D_r we get exactly the same result as obtained using the angular spectrum analysis (Equation 44). Thus simple energy conservation principles may be used to predict the Goos-Hänchen shift in this case.

We may examine explicitly the power flow behaviour in the xy plane using the type of calculation used in obtaining Figures 14 and 15. Figure 17(a) shows the overall power intensity and flux lines (Lai et al., 2000) for reflection off MnF_2 at frequency A, corresponding to the upper reststrahl region. The behaviour is similar to that predicted from Figure 16 (although in the present case the shift is negative). Thus, for $x > -0.01$ cm, the incident intensity is greater than the reflected intensity, so that the overall power flow is to the right. At $x \simeq -0.01$ cm, the incident and reflected beams cancel, whereas for $x < -0.01$ cm, the reflected beam dominates and the overall power flow is to the left. Flux continuity is thus preserved in the manner illustrated in Figure 16.

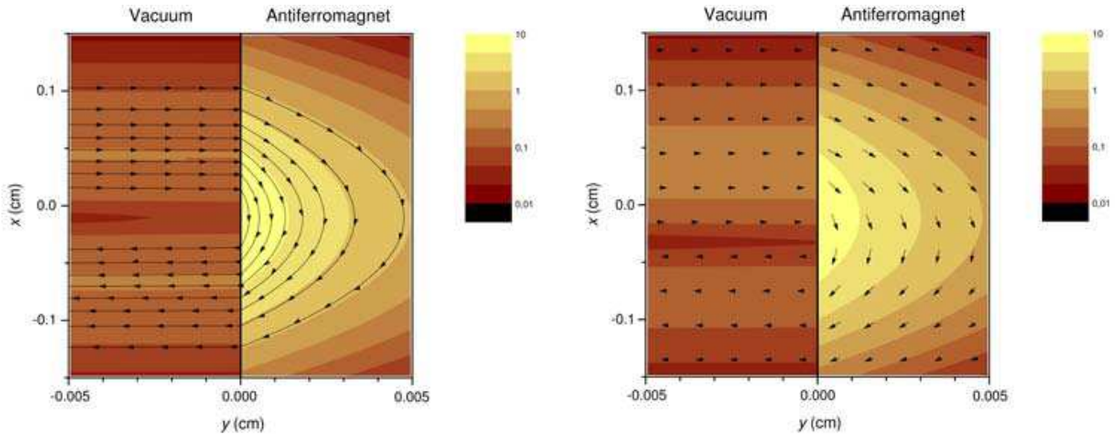

(a) Ignoring damping (b) Damping included

Fig. 17. Overall power intensity and flow for reflection off MnF_2 in an external magnetic field of 0.1 T in the upper reststrahl region (frequency A). After Lima et al. (2009).

Figure 17(b) shows power flow when damping is included. In this case the flux continuity argument no longer applies (hence we have not attempted to show continuous flux lines), but the overall behaviour is not significantly changed.

It is interesting to note that the power flow explanation of the normal incidence Goos Hänchen shift gives a very clear example of the breaking of time reversal symmetry by a static magnetic field. In the example shown in Figure 16, there is power flow along the positive x direction within the antiferromagnet, and the reflected beam is thus displaced in this direction. If, however, time reversal were applied to the reflected beam, so that it became a new incident beam, without reversing the direction of $\mathbf{B}_0$, the flow of energy within the antiferromagnet would not retrace its path along the negative x direction, but would once again flow along positive x, and there would be a further displacement of the reflected beam in this direction.

4.3.2 Bulk regions

The above power conservation principles used in analysing the normal incidence Goos-Hänchen shift in the reststrahl regions are based on the principle that all the incident energy

will be reflected back from the antiferromagnet surface. This is clearly not the case in the bulk regions. Furthermore, in the absence of damping, the power flow resulting from normally incident plane waves is transmitted normal to the surface, as seen in Figure 9(a). The reststrahl region analysis requires power flow parallel to the interface, so one might expect that there would be no lateral shift of the reflected beam in the bulk regions. The angular spectrum analysis, however, predicts that such a shift should occur in both the reststrahl and the bulk regions, so it is important to understand, in terms of energy flow, how such a shift is possible in the bulk regions.

In order to analyse the power flow, we once again take the example of reflection of a Gaussian beam and examine the power flow profile in the *xy* plane. The resulting overall power intensity and flux at the two bulk frequencies B and C are shown in Figure 18. Before analysing the lateral shift in any detail, it is worth noting that the profile of the power intensity within the antiferromagnet is different from that of the electric field amplitudes

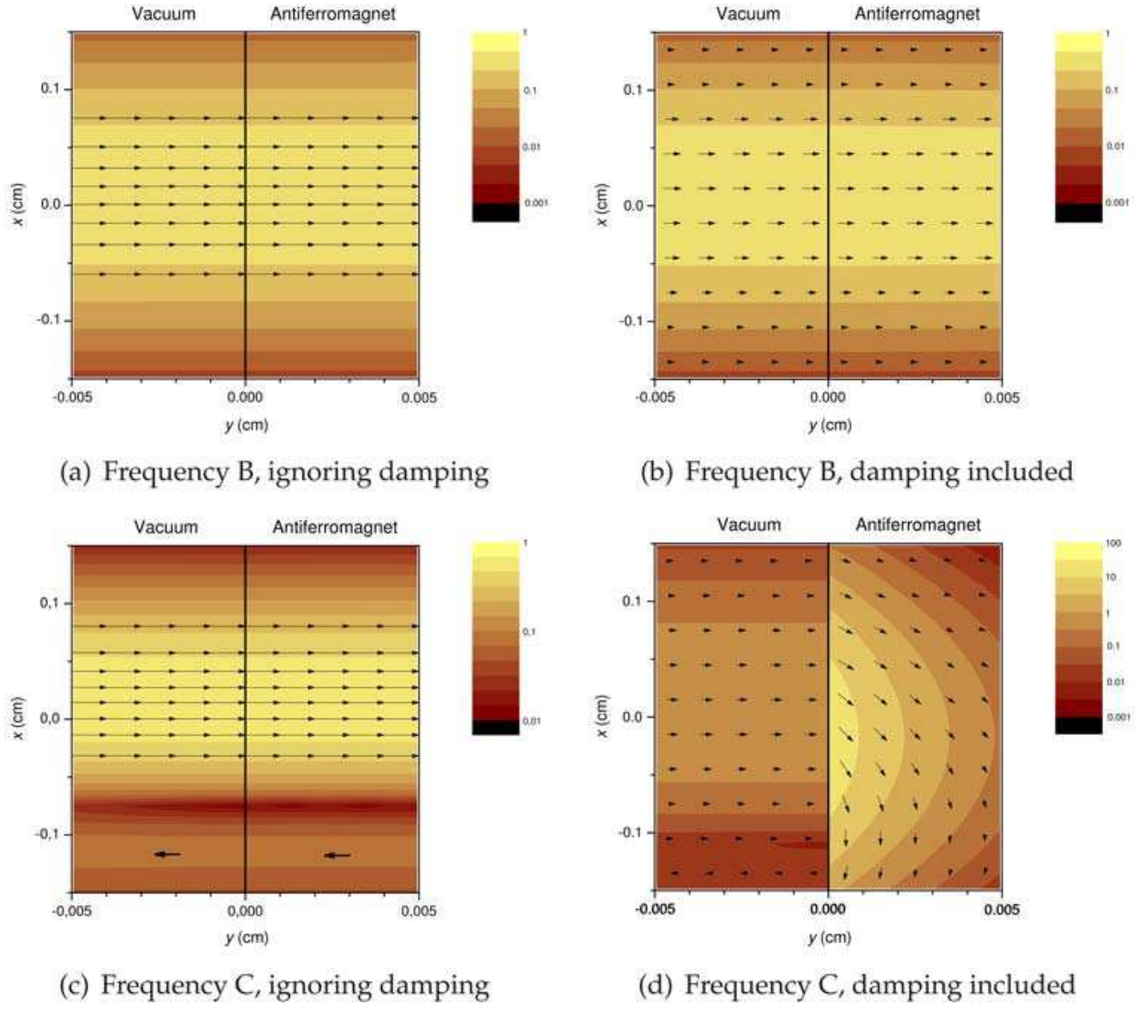

Fig. 18. Overall power intensity and flow for reflection off MnF_2 in an external magnetic field of 0.1 T in the bulk regions. Note that the arrows in the bottom half of (c) are simply intended to show the direction of power flow and are not a continuation of the flux lines in the upper part of the figure. After Lima et al. (2009).

shown in Figures 14 and 15. This is because the power intensity depends on the magnetic field component of the electromagnetic field as well as its electric field component. The magnetic field profile is in fact very different from that of the electric field (Lima et al., 2009), leading to a different power intensity profile.

At frequency B, ignoring damping (Figure 18(a)), overall power flow is to the right both in the vacuum region $y < 0$ and within the antiferromagnet $y > 0$, and remains perpendicular to the surface. There is flux continuity across the interface, as expected, and the overall profile is slightly displaced in the positive x direction with respect to the incident beam, which is centred at $x = 0$. We can understand this if we recall that the reflected beam is slightly displaced in the negative x direction and is less intense than the incident beam (see Figure 13(b)). The overall flux for $y < 0$, within the vacuum region, is the incident beam minus the reflected beam, so it is shifted in the positive x direction with respect to the pure incident beam. Flux continuity requires that this displacement is transferred to the transmitted beam, i.e. in the bulk regions the transmitted beam is displaced along x in the direction opposite to the displacement of the reflected beam. The behaviour in the presence of damping (Figure 18(b)) is not appreciably different.

At frequency C in the absence of damping (Figure 18(c)) the situation is similar to that at frequency B except that there is now a resultant power to the left for $x < -0.08$ cm^{-1}. This is related to the fact that the reflected beam is more intense than the incident beam at these values of x (see Figure 13(c)). This also means that there must be power flow to the left within the antiferromagnet. This presents an apparent problem since there is no obvious source for the associated energy. Nevertheless, detailed calculations of power flow several centimeters into the antiferromagnet show that a portion of the incident energy does indeed return to the left in this region (Lima et al., 2009). This is easier to see when damping is present (Figure 18(d)), in which case some of the incident energy returns to the left without penetrating a long distance into the antiferromagnet. In fact, in this case, the overall power flow is somewhat similar to that observed in the reststrahl regions. This is another illustration of the concept that, in the presence of damping, the bulk and reststrahl regions can be thought of as merging into one another.

In the above examples, frequency B (Figures 18(a) and 18(b)) can be regarded as representative of most of the bulk frequencies. Frequency C (Figures 18(c) and 18(d)), in contrast, displays rather peculiar behaviour particular to frequencies between the reststrahl region and the reflection minimum (see Figure 12).

5. Conclusions and future prospects

In this chapter we have examined various nonreciprocal effects associated with reflection of terahertz radiation off antiferromagnets. Of these effects, only nonreciprocity in the reflectivity has, to our knowledge, been investigated experimentally at the time of writing (Remer et al., 1986; Brown et al., 1994).

A simple, if slightly indirect, way of observing the nonreciprocal reflected phase has been suggested (Dumelow & Camley, 1996; Dumelow et al., 1998), and uses the configuration shown in Figure 19. Here, a dielectric layer is deposited onto the surface of an antiferromagnet and the overall reflectivity off the overall structure measured. In this setup, there is reciprocal reflection from the vacuum/dielectric interface, but the phase of the radiation reflected from the dielectric/antiferromagnet interface is nonreciprocal. Interference between these partial waves is thus nonreciprocal, leading to a nonreciprocal

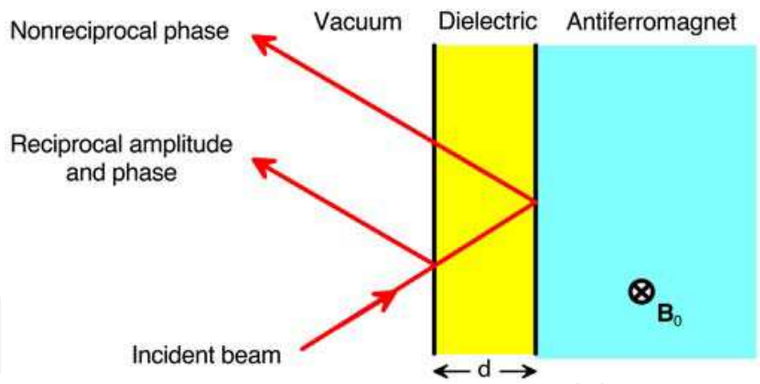

Fig. 19. Use of a dielectric layer for investigating nonreciprocal phase on reflection off an antiferromagnet.

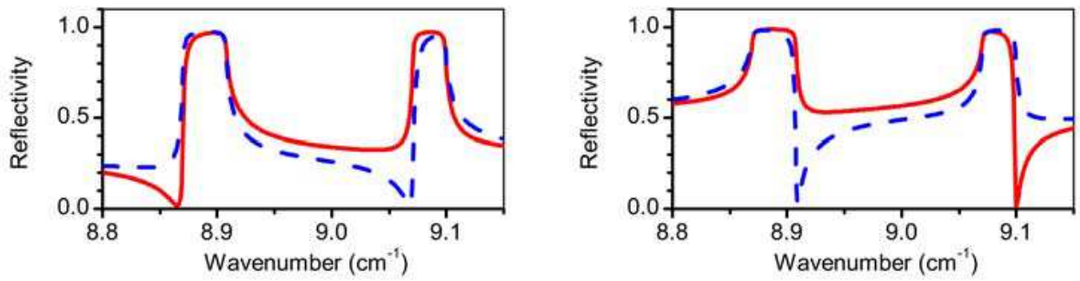

(a) $d = 10\mu$m (b) $d = 60\mu$m

Fig. 20. Calculated oblique incidence reflectivity spectrum off a Si/MnF_2 structure of the type shown in Figure 19 in an external field of $B_0 = +0.1$ T (solid curves) and $B_0 = -0.1$ T (dashed curves).

overall reflectivity which depends on the dielectric layer thickness, as shown in Figure 20. This is true even when the reflectivity off the pure antiferromagnet is close to reciprocal, as is the case for MnF_2.

The discussion of nonreciprocity in the power flow is concerned with power flow behaviour within the interior of an antiferromagnet. Obviously it is not straightforward to measure this experimentally. It appears more reasonable to investigate the effect of this nonreciprocal power flow on the radiation interacting with a finite sized sample of a given shape. The analysis presented in this chapter does not extend to this type of system, since the antiferromagnet is considered to be infinite along x. However, other techniques such as the finite difference time domain (FDTD) method should help clarify the expected behaviour.

The lateral shift predicted in the case of reflection of a finite beam off an antiferromagnet should in principle be measurable given a suitable coherent source such as a far infrared laser (Rosenbluh et al., 1976), backward wave oscillator (Dobroiu et al., 2004), or YIG oscillator with frequency multiplied output (Kurtz et al., 2005). In order to observe the normal incidence shift, a beam splitting arrangement appears necessary. It is also, however, important to consider the effect at oblique incidence, both theoretically and experimentally. In this case the effect should be observable directly without the use of a beamsplitter.

In this chapter we have only discussed phenomena in the Voigt configuration with the external field aligned along the anisotropy axis, deliberately avoiding the more complicated configurations in which the external field makes an angle with the anisotropy field (Almeida

& Mills, 1988), or in which these axes are not perpendicular to the plane of incidence. However, we should point out that theoretical works on the reflected amplitude and phase do exist for more complex geometries (Stamps et al., 1991; Dumelow et al., 1998), and, in the case of reflectivity, there is some experimental work (Abraha et al., 1994; Brown et al., 1995).
Finally, we stress that, although we have concentrated on reflection off antiferromagnets in this chapter, the basic priciples involved stem from the form of the permeability tensor given in Equation 8. However, there are other types of material, such as ferromagnets or ferrimagnets, that also have a gyromagnetic permeability of this form. We therefore expect similar phenomena for these materials, although some of the symmetry arguments have to be looked at in a slightly different way since, in general, such materials have their own internal macroscopic magnetic field. One can also have a dielectric tensor of this form, such as that associated with magnetoplasma excitations. In this case, p-polarisation radiation should give results similar to those presented here for s-polarisation reflection off antiferromagnets (Remer et al., 1984).

6. Acknowledgments

This work was partially financed by the Brazilian Research Agency CNPq (projects Universal 482238/2007-0, CT-ENERG 554889/2006-4, and CNPq-Rede NanoBioestruturas 555183/2005-0).

7. References

Abraha, K., Brown, D. E., Dumelow, T., Parker, T. J. & Tilley, D. R. (1994). Oblique incidence far-infrared reflectivity study of the uniaxial antiferromagnet fef_2, *Phys. Rev. B* 50(10): 6808–6816.

Abraha, K. & Tilley, D. R. (1996). Theory of far infrared properties of magnetic surfaces, films and superlattices, *Surf. Sci. Rep.* 24(5-6): 129-222.

Almeida, N. S. & Mills, D. L. (1988). Dynamical response of antiferromagnets in an oblique magnetic field: Application to surface magnons, *Phys. Rev. B* 37(7): 3400–3408.

Artmann, K. (1948). Berechnung der seitenversetzung des totalrelektierten strahles, *Ann. Physik* 437: 87–102.

Born, M. &Wolf, E. (1980). *Principles of Optics*, sixth edn, Pergamon Press, Oxford.

Brown, D. E., Dumelow, T., Parker, T. J., Abraha, K. & Tilley, D. R. (1994). Nonreciprocal reflection by magnons in FeF_2: a high resolution study, *Phys. Rev. B* 49(17): 12266–12269.

Brown, D. E., Dumelow, T., Parker, T. J., Abraha, K. & Tilley, D. R. (1995). Far infrared reflectivity off FeF_2, *J. Magn. Magn. Mater.* 140-144: 181–182.

Brown, D. E., Dumelow, T., Parker, T. J., Jensen, M. R. F. & Tilley, D. R. (1998). A high resolution fourier transform spectrometer for far infrared magneto-optic spectroscopy of magnetic materials, *Infrared Physics and Technology* 40: 219–230.

Camley, R. E. (1987). Nonreciprocal surface modes, *Surf. Sci. Rep.* 7(3-4): 103–188.

Dobroiu, A., Yamashita, M., Ohshima, Y. N., Morita, Y., Otani, C. & Kawase, K. (2004). Terahertz imaging system based on a backward-wave oscillator, *Appl. Opt.* 43(30): 5637– 5646.

Dötsch, H., Bahlmann, N., Zhuromskyy, O., Hammer, M., Wilkens, L., Gerhardt, R., Hertel, P. & Popkov, A. F. (2005). Applications of magneto-optical waveguides in integrated optics: review, *J. Opt. Soc. Am. B* 22(1): 240–253.

Dumelow, T. & Camley, R. E. (1996). Nonreciprocal reflection of infrared radiation from structures with antiferromagnets and dielectrics, *Phys. Rev. B* 54(17): 12232–12237.

Dumelow, T., Camley, R. E., Abraha, K. & Tilley, D. R. (1998). Nonreciprocal phase behavior in reflection of electromagnetic waves from magnetic materials, *Phys. Rev. B* 58(2): 897– 908.

Dumelow, T. & Oliveros, M. C. (1997). Continuum model of confined magnon polaritons in superlattices of antiferromagnets, *Phys. Rev.* B 55(2): 994-1005.

Goos, F. & Hänchen, H. (1947). Ein neuer und fundamentaler versuch zur totalreflexion, *Ann. Physik* 436(6): 333–346.

Horowitz, B. R. & Tamir, T. (1971). Lateral displacement of a light beamat a dielectric interface, *J. Opt. Soc. Am.* 61(5): 586–594.

Kurtz, D., Crowe, T., Hesier, J., Porterfield, D., Inc, V. & Charlottesville, V. (2005). Frequency domain terahertz spectroscopy, *Infrared and Millimeter Waves and 13th International Conference on Terahertz Electronics, 2005.*, Vol. 1, pp. 76–77.

Lai, H. M., Kwok, C. W., Loo, Y. W. & Xu, B. Y. (2000). Energy-flux pattern an the Goos-Hänchen effect, *Phys. Rev. E* 62(5): 7330–7339.

Landau, L. D. & Lifshitz, E. M. (1984). *Electrodynamics of Continuous Media*, second edn, Pergamon Press, Oxford.

Leung, P. T., Chen, Z. W. & Chiang, H.-P. (2007). Large negative Goos-Hänchen shift at metal surfaces, *Opt. Commun.* 276(2): 206–208.

Lima, F., Dumelow, T., Albuquerque, E. L. & da Costa, J. A. P. (2009). Power flow associated with the Goos-Hänchen shift of a normally incident electromagnetic beam reflected off an antiferromagnet, *Phys. Rev. B* 79(15): 155124.

Lima, F., Dumelow, T., da Costa, J. A. P. & Albuquerque, E. L. (2008). Lateral shift on normal incidence reflection off an antiferromagnet, *Europhys. Lett.* 83(1): 17003.

Lotsch, H. K. V. (1970). Beam displacement at total reflection: the Goos-Hänchen effect, *Optik* 32: 116,189,299,553.

McGuirk, M. & Carniglia, C. K. (1977). An angular spectrum approach to the Goos-Hänchen shift, *J. Opt. Soc. Am.* 67(1): 103–107.

Mills, D. L. & Burstein, E. (1974). Polaritons: the electromagnetic modes of media, *Rep. Prog. Phys.* 37(7): 817-926.

Potton, R. (2004). Reciprocity in optics, *Rep. Progr. Phys.* 67(5): 717–753.

Remer, L., Lüthi, B., Sauer, H., Geick, R. & Camley, R. E. (1986). Nonreciprocal optical reflection of the uniaxial antiferromagnet MnF_2, *Phys. Rev. Lett.* 56(25): 2752–2754.

Remer, L., Mohler, E., Grill, W. & Lüthi, B. (1984). Nonreciprocity in the optical reflection of magnetoplasmas, *Phys. Rev. B* 30(6): 3277–3282.

Renard, R. H. (1964). Total reflection: a new evaluation of the Goos-Hänchen shift, *J. Opt. Soc. Am.* 54(10): 1190–1197.

Rosenbluh, M., Temkin, R. J. & Button, K. J. (1976). Submillimeter laser wavelength tables, *Appl. Opt.* 15(11): 2635–2644.

Scott, R. Q. &Mills, D. L. (1977). Propagation of surface magnetostatic waves on ferromagnetic crystal structures, *Phys. Rev. B* 15(7): 3545–3557.

Stamps, R. L., Johnson, B. L. & Camley, R. E. (1991). Nonreciprocal reflection from semi-infinite antiferromagnets, *Phys. Rev. B* 43(4): 3626–3636.

Wild, W. J. & Giles, C. L. (1982). Goos-Hänchen shifts from absorbing media, *Phys. Rev. A* 25(4): 2099–2101.

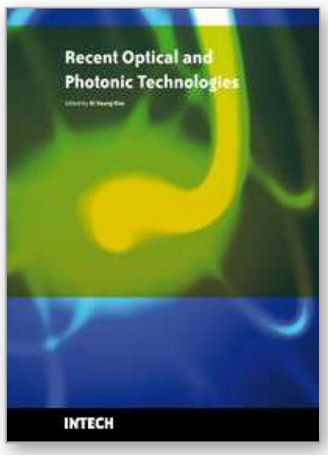

Recent Optical and Photonic Technologies

Edited by Ki Young Kim

ISBN 978-953-7619-71-8
Hard cover, 450 pages
Publisher InTech
Published online 01, January, 2010
Published in print edition January, 2010

Research and development in modern optical and photonic technologies have witnessed quite fast growing advancements in various fundamental and application areas due to availability of novel fabrication and measurement techniques, advanced numerical simulation tools and methods, as well as due to the increasing practical demands. The recent advancements have also been accompanied by the appearance of various interdisciplinary topics. The book attempts to put together state-of-the-art research and development in optical and photonic technologies. It consists of 21 chapters that focus on interesting four topics of photonic crystals (first 5 chapters), THz techniques and applications (next 7 chapters), nanoscale optical techniques and applications (next 5 chapters), and optical trapping and manipulation (last 4 chapters), in which a fundamental theory, numerical simulation techniques, measurement techniques and methods, and various application examples are considered. This book deals with recent and advanced research results and comprehensive reviews on optical and photonic technologies covering the aforementioned topics. I believe that the advanced techniques and research described here may also be applicable to other contemporary research areas in optical and photonic technologies. Thus, I hope the readers will be inspired to start or to improve further their own research and technologies and to expand potential applications. I would like to express my sincere gratitude to all the authors for their outstanding contributions to this book.

INTECH
open science | open minds

InTech Europe
University Campus STeP Ri
Slavka Krautzeka 83/A
51000 Rijeka, Croatia
Phone: +385 (51) 770 447
Fax: +385 (51) 686 166

InTech China
Unit 405, Office Block, Hotel Equatorial Shanghai
No.65, Yan An Road (West), Shanghai, 200040, China
中国上海市延安西路65号上海国际贵都大饭店办公楼405单元
Phone: +86-21-62489820
Fax: +86-21-62489821

IntechOpen

IntechOpen